Supporting Information

Hierarchical Integrated 3D Hollow MnS@MoS_2 Microcube *via* Template-Controlled Synthesis for Asymmetric Supercapacitors

Qiannan Zhou,[§ab] Wei Li,[§b] Huizhong Xu,[a] Mengyou Gao,[c] Xiaochen Dong,[d] and Jianjian Lin[*a]

[a] *Shandong Key Laboratory of Biochemical Analysis, College of Chemistry and Molecular Engineering, Qingdao University of Science and Technology, Qingdao 266042, China.*

[b] *Engineering Research Center of High Performance Polymer and Molding Technology, Qingdao University of Science and Technology, Qingdao 266042, China.*

[c] *College of Automation and Electronic Engineering, Qingdao University of Science and Technology, Qingdao 266042, China.*

[d] *Key Laboratory of Flexible Electronics (KLOFE) & Institute of Advanced Materials (IAM), Nanjing Tech University (NanjingTech), 30 South Puzhu Road, Nanjing, 211800, China.*

*Corresponding author. E-mail: Jianjian_Lin@qust.edu.cn

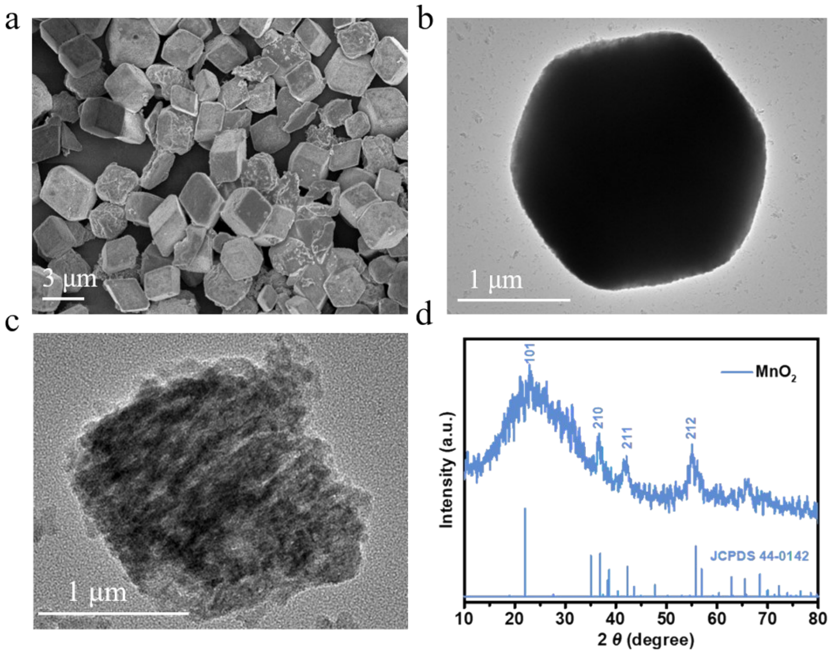

Figure S1. (a, b) SEM and TEM images of $MnCO_3$. (c, d) TEM image and XRD pattern of hollow MnO_2.

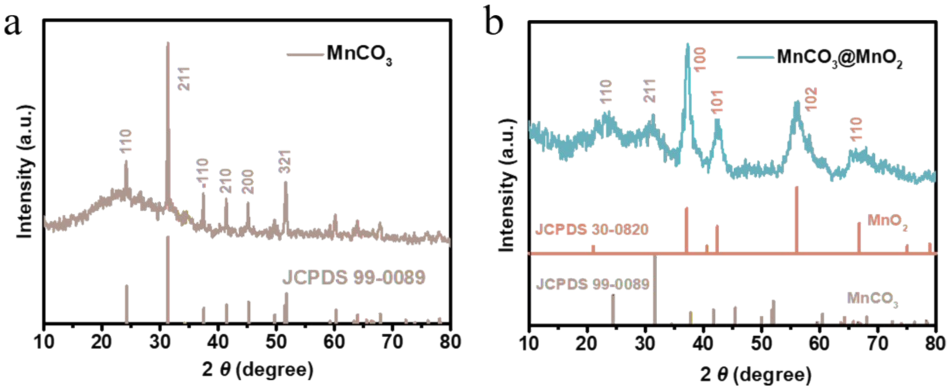

Figure S2. The XRD pattern of (a) $MnCO_3$ and (b) $MnCO_3@MnO_2$.

The peak at 23° and 33° in the XRD patterns (Figure S2b) are matched to the (110) and (211) crystal planes of $MnCO_3$ (JCPDS 99-0089), which confirmed the existence of intermediates. This XRD pattern (Figure S2) indicated the $MnCO_3$ transformed into the $MnCO_3@MnO_2$ after the calcination and the as-synthesized composite was the basis of H^+ etching into hollow-cube through.

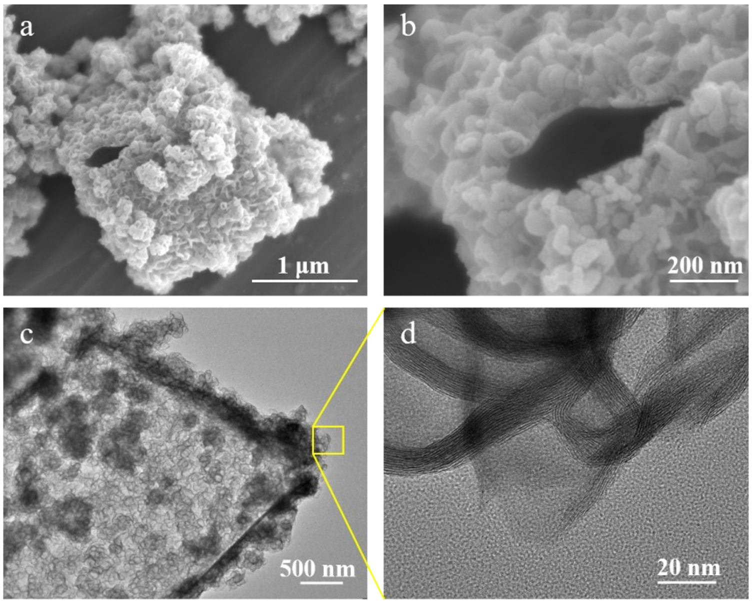

Figure S3. The SEM and TEM images of $MnS@MoS_2$.

As shown in Figure 1d and Figure S3c, the TEM images of $MnS@MoS_2$ proved the existence of hollow structure. The hollow MnS microcube was wrapped by the MoS_2 nanosheets. Besides, the structural features of MoS_2 nanosheets can be seen from the enlarged TEM image of edges (Figure S3d).

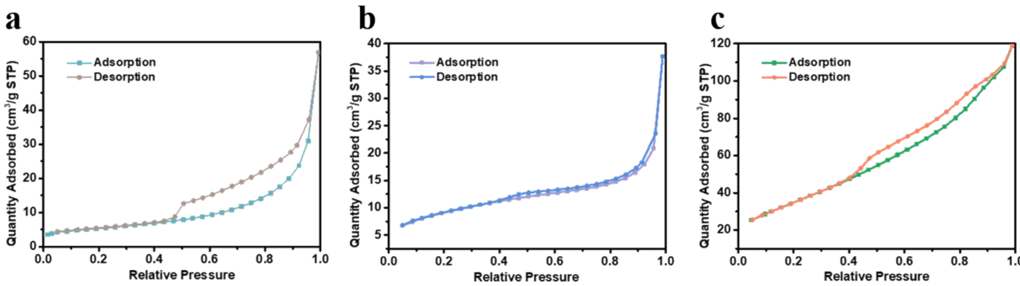

Figure S4. The N_2 ab-/desorption isotherm curves of (a) $MnCO_3$, (b) MnO_2 and (c) $MnS@MoS_2$ composite.

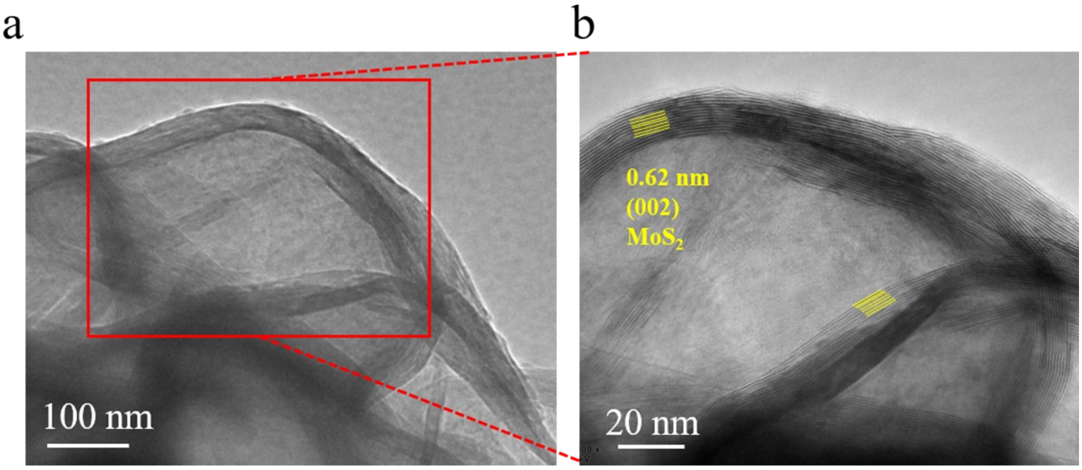

Figure S5. (a) TEM images of edge MoS_2. (b) Enlarged TEM image of a.

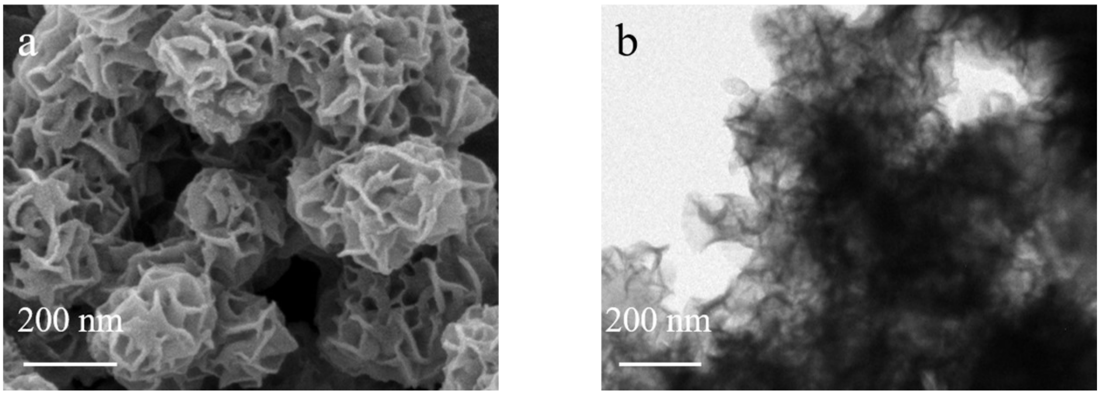

Figure S6. (a, b) SEM and TEM images of pure MoS_2.

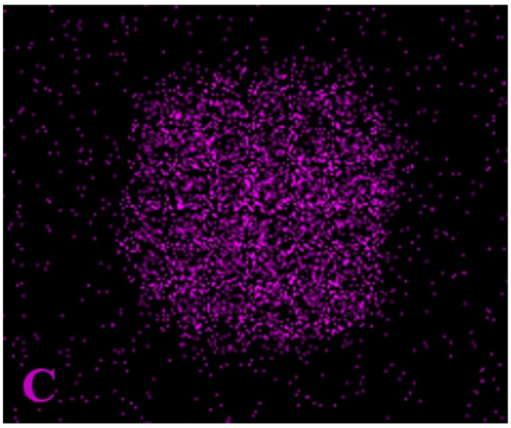

Figure S7. EDS mapping of C elements.

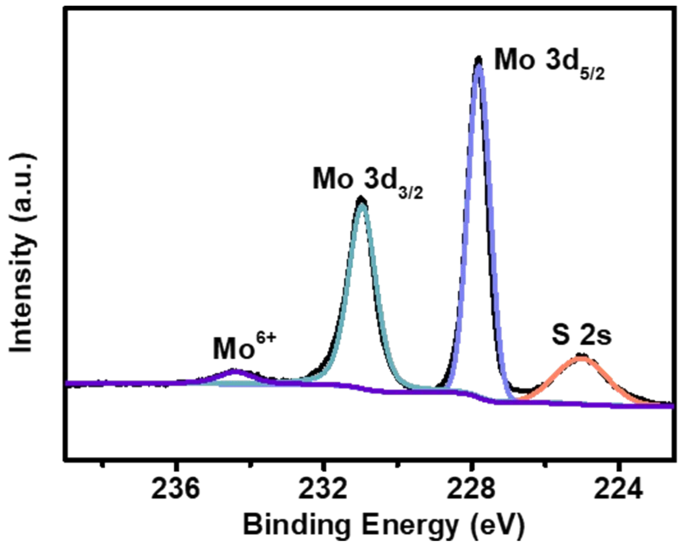

Figure S8. The high-resolution Mo XPS spectra of MoS_2.

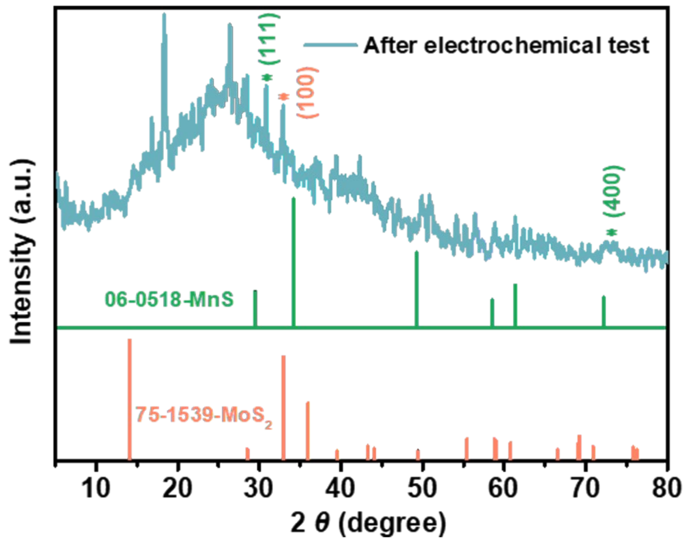

Figure S9. The XRD pattern of MnS@MoS_2 after electrochemical test.

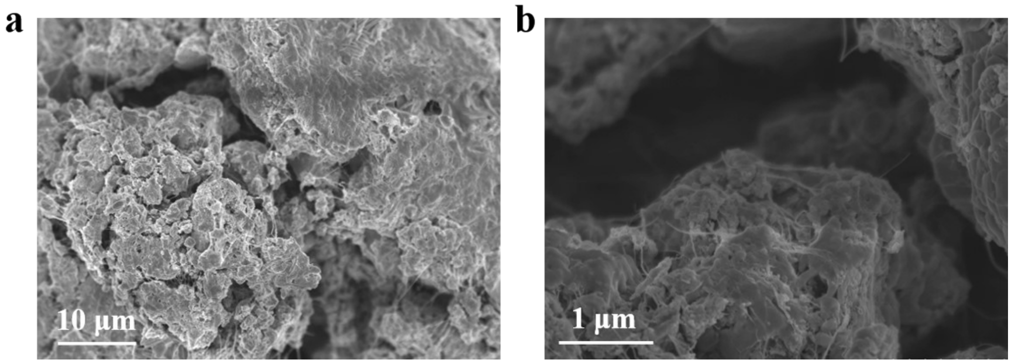

Figure S10. The SEM images of $MnS@MoS_2$ after electrochemical test.

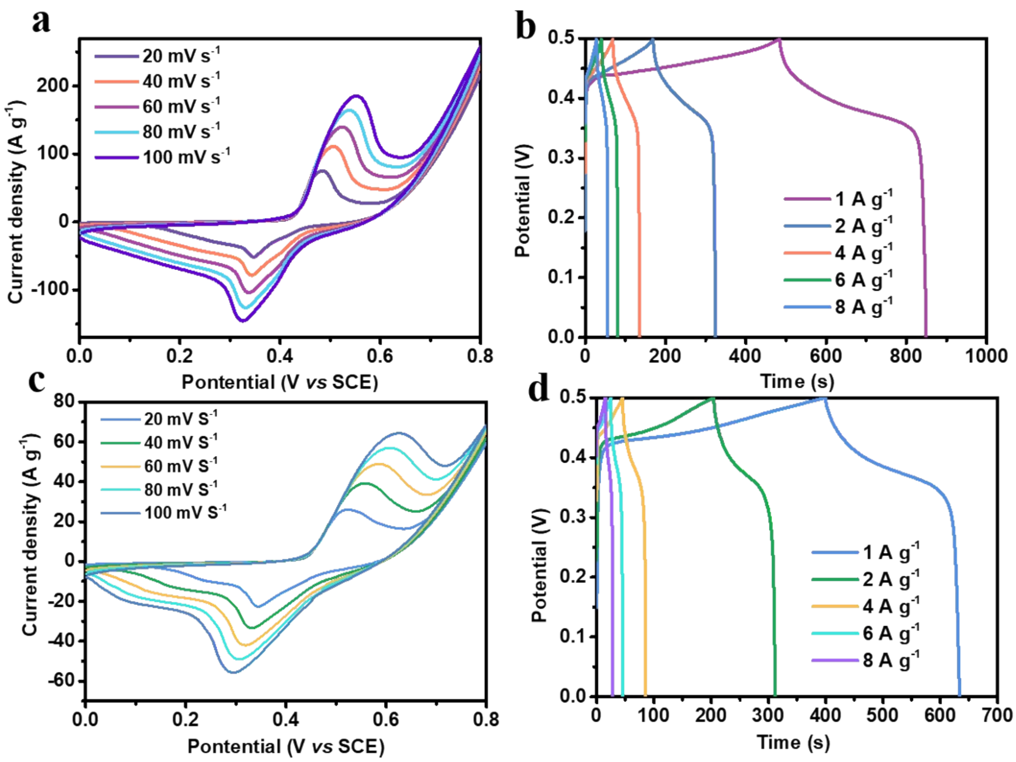

Figure S11. (a) CV curves of MoS_2 at various scan rates. (b) GCD curves of MoS_2 at various current densities. (c) CV curves of MnS at various scan rates. (d) GCD curves of MoS_2 at various current densities.

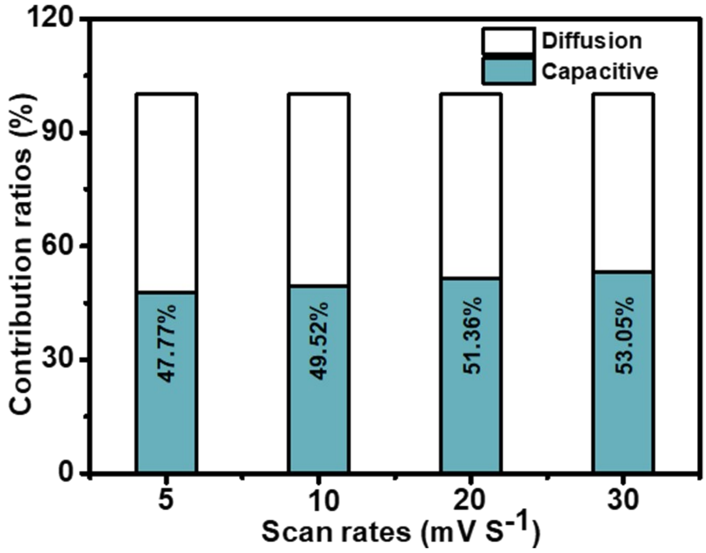

Figure S12. The capacitive contributions of $MnS@MoS_2$ at 5-30 mV s^{-1}.

The contribution of different charge storage mechanism can be further characterized by the data at the scan rates of 5-30 mV s^{-1}. The contribution of surface capacitive process increased with the scan rates increasing.

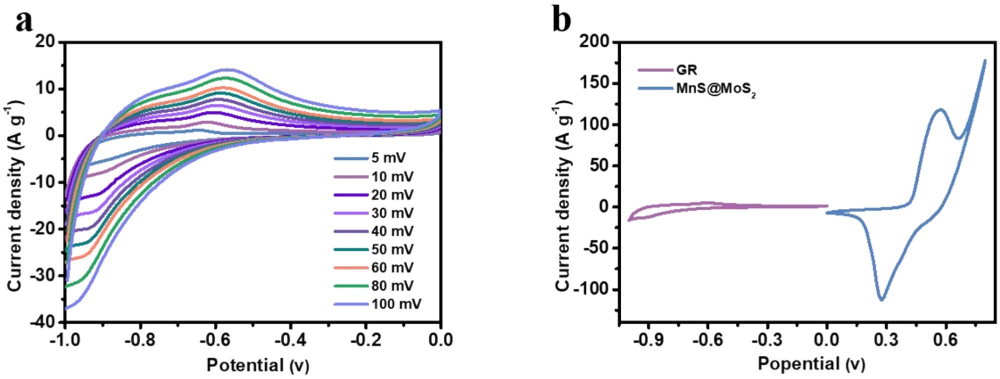

Figure S13. (a) CV curves of the GR at 5–100 mV s^{-1}. (b) CV curves collected for GR and $MnS@MoS_2$ electrodes at a scan rate of 50 mV s^{-1}.

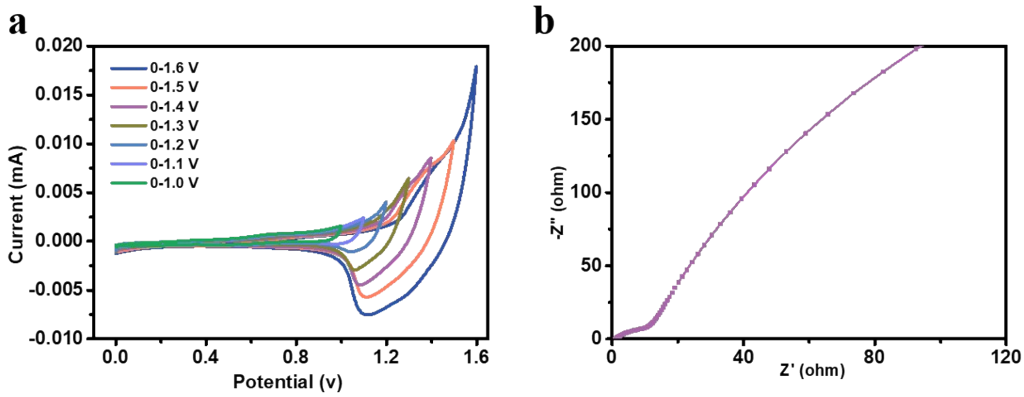

Figure S14. (a) CV curves of the $MnS@MoS_2$//GR at various potential windows of 20 mV s^{-1}. (b) EIS of $Mn@MoS_2$//GR device.

Table S1 Comparison with previous reported asymmetric supercapacitors device

Electrode material	Energy density	Power density
Ni-Co-S@MnS	20.5	2000
MnO_2@ppy	23	1800
MnS microfiber	42.7	1200
MnS nanocrystal	24.9	5946
This work	65/29	1600/6400